This is a peer-reviewed, accepted author manuscript of the following research article: Ye, J., Quan, G., Yun, X., Guo, X., & Chen, J. (2022). An improved and robust finite element model for simulation of thin-walled steel bolted connections. *Engineering Structures*, *250*, [113368]. https://doi.org/10.1016/j.engstruct.2021.113368

An improved and robust finite element model for simulation of thin-walled steel bolted connections

Jun Ye[1,2], Guan Quan[3*], Xiang Yun[2], Xi Guo[2], Ju Chen[1]

1 College of Civil Engineering and Architecture, Zhejiang University, Hangzhou, 310058, China

2 Department of Civil & Environmental Engineering, Imperial College London, London, SW7 2AZ, UK

3 School of Civil Engineering and Surveying, University of Portsmouth, Portsmouth, PO1 3AH, UK

Abstract: Thin-walled cold-formed steel (CFS) structures are widely used in low-storey buildings and are seeing increased applications in multi-storey buildings as well as long-span structures. The bolted connection is one of the most common types of fasteners employed in CFS structures. The bolt slippage and load-bearing mechanism in CFS connections have a significant influence on the structural behaviour of cold-formed steel construction assemblies, which are typically numerically simulated using spring/connector elements. However, the determination of input parameters for the spring/connector elements generally requires load-deformation characteristics obtained from physical tests of lap joints, which are costly and time-consuming. Moreover, the use of spring/connector elements fails to explicitly capture the bolt bearing behaviour, resulting in inaccuracy in the simulation of CFS connections. In this paper, an accurate, efficient and robust numerical method that can fully replicate the behaviour of CFS connections considering both the effects of bolt slippage and bearing has been introduced. In the proposed numerical methodology, the cold-formed plates are modelled using the conventional shell elements, while a number of solid elements are introduced around the bolt holes, enabling the bolt-plate interaction to be explicitly accounted for, with contact pairs defined between the bolts and their surrounding solid element surfaces. The proposed numerical method could find a convergence solution using dynamic implicit solver in the

general-purpose finite element (FE) software ABAQUS. Good agreement between the FE models using the proposed method and the available test results of CFS bolted connections were achieved, which sheds light on the promising application of the proposed method for simulating CFS assembled using bolted connections.

Keywords: Bolted connections, Built-up sections, Cold-formed steel, Computational modelling, Numerical simulation

1 Introduction

Cold-formed steel (CFS) members are widely used in the construction industry due to their high strength-to-weight ratios and possibility for the fabrication of complex shapes, with various cross-section profiles achievable. CFS members are widely used in low-rise buildings and are seeing increased applications in multi-storey buildings and long-span structures. A number of codes of practice [1-3] have been developed for the design of CFS structures.

The most widely used types of connections include bolted joints, screw fasteners [4, 5], spot welds, blind rivets, power actuated fasteners [6-8] and clinching connections [9]. Connections are regarded as an important component in CFS structures and their characteristics can have a significant impact on the structural behaviour of the connected members and, eventually, the whole system. It has been found that the resistance of a cold-formed steel structure is largely dependent on the bolt configurations of connections under normal loading conditions [10-12]. Moreover, under seismic loading, Sabbagh *et al.* [13] found that web buckling adjacent to the first line of the bolts in the through-plate beam-to-column connections was the main reason to cause premature loss of the strength for the connected CFS beams. Sabbagh *et al.* [14] and Sato and Uang [15] concluded that bolted connections can be designed to provide improved ductility and energy dissipation capacity through initial slippage and bearing action. More recently, Ye

et al. [16] revealed the influence of bolt slippage on the hysteretic behaviour of connections and thus affecting the seismic performance of cold-formed steel frames.

The experimental investigations on CFS connections [17-28] are deemed necessary and practical for design at the component level. When the design is advanced to a performance-based full-structural level, complexities will arise and developing a precise modelling technique to simulate the structural behaviour of CFS structures become highly necessary.

And very often, experiments are carried out to provide a validation database to support the development of computational modelling techniques. However, the complex interaction between the CFS members and the fasteners, combined with their intricate geometry and material nonlinearity, renders the numerical modelling of CFS connections a difficult task.

Shell elements are conventionally used for the finite element (FE) modelling of CFS plated elements [29, 30] as they are able to precisely capture the cross-section level instabilities and material nonlinearity, while solid elements are typically used for the simulation of fasteners. The fastener-to-plate interaction is typically simulated by establishing the edge-to-surface contact between the solid elements of fasteners and the surrounding shell elements of the plates, as illustrated in Fig. 1(a). However, such models are difficult to accurately capture the stiffness caused by the bearing action between the bolt hole surfaces of CFS plates and the shank of fasteners. A more reliable modelling approach is to use solid elements for both the fasteners and CFS plates, enabling surface-to-surface contact to be established, as shown in Fig. 1(b), but modelling the thin-walled CFS plates with solid elements results in substantial computational cost and inaccuracy [31].

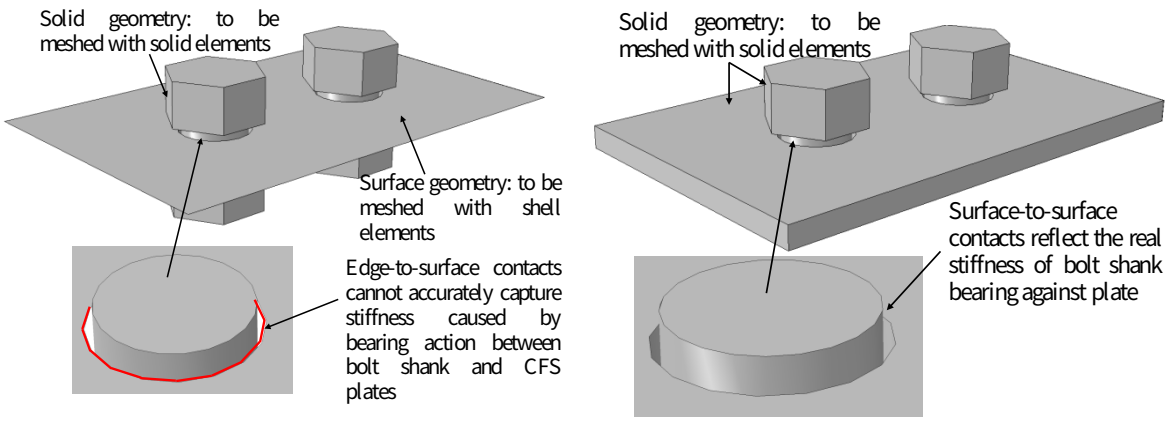

(a) (b)

Fig. 1. Traditional FE modelling techniques for considering bearing action between bolt shank and CFS plate (a) edge-to-surface contact and(b) surface-to-surface contact.

To overcome the aforementioned drawbacks, non-linear springs or connector elements are typically employed to mimic the interaction behaviour between bolts and CFS plates, while the CFS plates are modelled using the computationally efficient shell elements, as shown in Fig. 2. By doing so, the contact behaviour within the connections can be reflected by the non-linear springs or connector elements. This technique of modelling fasteners was commonly used a decade ago when Lim and Nethercot [18] developed a numerical model to study the structural behaviour of cold-formed steel portal frame systems. In their FE models, the bolts were represented by nonlinear spring elements anchored on the fastener points of each plate, as illustrated in Fig. 2(b). Other researchers [19, 32-35] also adopted the same methodology for the simulation of CFS fasteners. However, this method may result in excessive membrane deformation at the two anchor points of the spring elements. To address this problem, an improved approach, widely used nowadays, was proposed by using the connector elements to simulate the interaction behaviour between bolts and CFS plates, as shown in Fig. 2(c). In this method, the endpoints of connector elements were coupled to their corresponding plate mesh nodes nearby the centre of bolt holes within a defined influence radius through the kinematic

coupling, as illustrated in Fig. 2(c). This method successfully reduced the membrane deformation at the connector ends and led to more accurate simulation results. By employing the connector elements in their numerical models, Sabbagh *et al.* [14] investigated the cyclic behaviour of CFS bolted connections. Ye *et al.* [16, 36-38] successfully replicated the behaviour of bolted connections subjected to both monotonic and cyclic loadings using this modelling methodology. Moreover, Ye *et al*. [16] and Shahini *et al.* [39] adopted this approach to investigate the CFS moment-resisting connections with a bolting friction-slip mechanism for seismic design applications. More recently, Wald and his co-authors [40-42] proposed a new method named Component Based Finite Element Method (CBFEM) to analyse and design connections of steel structures. The CBFEM decomposes a steel joint into a number of separated components (i.e. steel plates, welds, bolts and anchors) and employs different analysis models to for the separated components (i.e. shell elements for all plates, special constraints for welds, and nonlinear spring elements for bolts and anchors). Compared to the commonly used Component Model and the sophisticated 3D Finite Element Model using solid elements, CBFEM achieves a balance between effectiveness and efficiency, while being able to provide sufficient information (e.g. stresses and strains of individual components) for designers to evaluate the structural behaviour and safety of the joint. The CBFEM also provides a robust and practical tool for analysing more complex joints which are out of the scope of the current design codes of practice. A large number of validation studies has been carried out [43-45], highlighting the accuracy and reliability of the CBFEM.

Despite all the aforementioned efforts made to simulate the CFS connections with increasingly improved accuracy, the determination of input parameters for use in both the spring and the connector elements relies largely on physical tests of lap shear joints, which are time-consuming and costly.

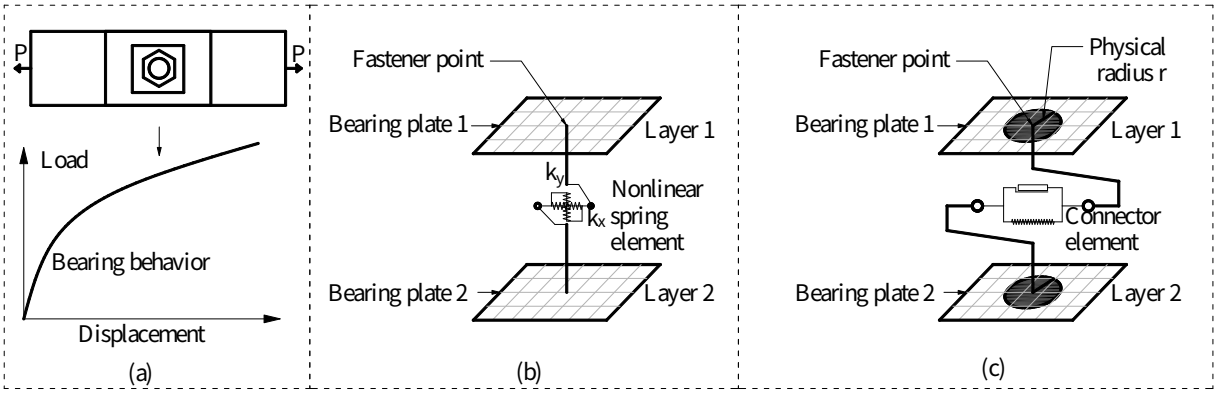

Fig. 2. Illustration of FE modelling methodologies for CFS bolted connections using spring or connector elements (a) load-displacement characteristics of bolt connections obtained from tests; (b) FE models using spring elements; and (c) FE models using connector elements.

The present study aims to develop an improved and robust numerical approach that can accurately replicate the behaviour of bolted connections subjected to both monotonic and cyclic loadings. Similar to the conventional modelling approach, the shell elements are used to model the majority part of the CFS plates, while a number of solid elements are employed around the bolt holes, with the aim to allow for an accurate definition of the contact interaction between the shank of bolts (also modelled using solid elements) and the surface of bolt holes. The proposed numerical modelling methodology is capable of applying pretension to the bolts, considering geometric and material nonlinearities as well as accounting for the effect of bolt slippage. The FE models can be performed using the ABAQUS standard dynamic implicit solver, which helps the convergence and generates reliable results without the need to check parameters, such as the loading speed and energy balance, which is normally required if the models are numerically solved using dynamic explicit solver. The proposed numerical modelling methodology has been validated by comparisons between the numerical results and the representative physical test data reported in different literature, confirming that the proposed simulation approach can accurately capture the structural behaviour of bolted CFS

connections. The proposed numerical approach is found to be accurate, efficient and robust to be used for the simulation of different types of CFS structures assembled using bolted connections.

2 Key characteristics of the proposed numerical approach

In this paper, a novel modelling technique is proposed, with the aim to accurately capture the structural behaviour of CFS members with bolted connections. The numerical simulation is established based on ABAQUS [46], where shell elements are dominantly used to model the CFS components, while a small number of solid elements are employed around the bolt holes to facilitate the establishment of surface-to-surface contact between the bolt shank and the surface of the bolt hole. The proposed modelling technique is able to explicitly consider the effects of bolt slippage and bolt bearing (i.e. bolt shank in contact with the bole hole) on the structural performance of CFS structures, with both computational efficiency and simulation accuracy. The key characteristics of the proposed numerical modelling technique are presented in this section.

2.1 Elements and contact properties

Shell elements are typically utilised to model thin-walled CFS structural components, as they are able to explicitly capture cross-section level instabilities and are more computationally efficient than solid elements. However, when comes to the numerical modelling of connections in CFS structures, solid elements can provide a more detailed and accurate replication of the localised bolt bearing behaviour. Therefore, by combining the merits of both shell and solid elements, a more efficient modelling technique for the simulation of bolt connections in CFS structures is proposed herein. Shell elements are dominantly used to simulate the CFS plates, while solid elements are employed to model a small block region of the CFS plates located

around the bolt hole where contact pressure is concentrated. Bolts are also modelled using solid elements and surface-to-surface contacts between the bolt shank and the bolt hole surfaces of the contacted block plates (also modelled using solid elements) are defined. It is worth noting that the size of the block plates around the bolt hole should be sufficiently large to cover the area of the bolt nut/head and the area where the bolt hole elongation caused by the bearing effect is pronounced.

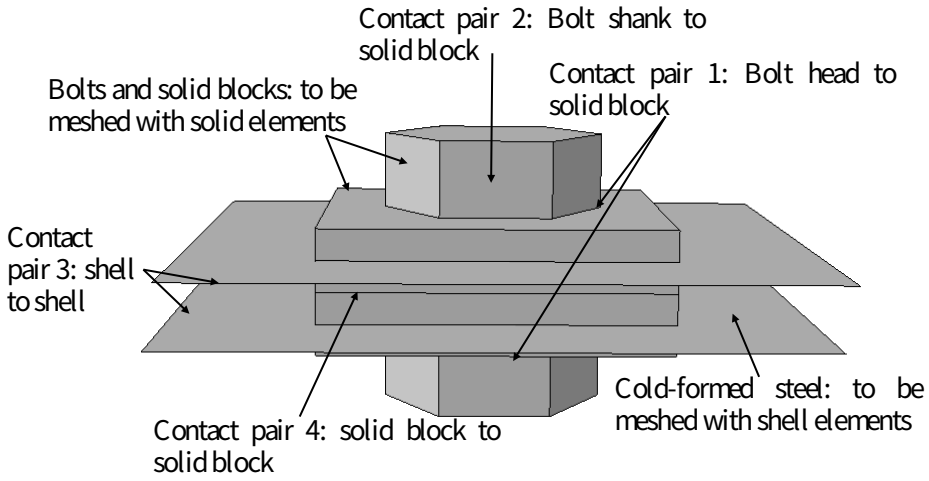

Fig. 3. Illustration of the proposed numerical modelling technique of using both shell and solid elements in a typical shear lap connection model.

The contact interactions between the bolts and the block plates and between the contacted block plates are modelled using surface-to-surface contact elements, as shown in Fig. 3, with the Coulomb friction coefficient μ = 0.15 [47] in the tangential direction. The contact normal to the surface is defined as "Hard-contact" to prevent penetration of the surfaces.

2.2 Solver scheme

The complex contact settings as well as the material nonlinearly of cold-formed steel make the static solver in ABAQUS [46] difficult to find a convergent solution or trace the post-ultimate response. Therefore, the dynamic implicit solver is recommended to solve FE models of bolt

connections using the proposed modelling technique. The implicit integration schemes usually give acceptable solutions using automatic time incrementation.

2.3 Bolt pretension

For CFS bolted connections, where clearance between the bolt hole and the bolt shank exists prior to testing, as illustrated in Fig. 4, (a), slippage occurs when the applied loads overcome the bolt-slip resistance, the value of which is related to the roughness of the contacting surfaces (i.e. the friction coefficient μ) and the bolt pretension P_b (applied via the bolt head using a torque wrench). For connections in which the clearance between the bolt hole and the bolt shank is eliminated prior to loading, the load-deformation curve is characterised by a bearing deformation curve with no slippage, as shown in Fig. 4(b). However, the slippage is apparent in the load-displacement curves obtained from connections in which the clearance between the bolt hole and the bolt shank exists prior to loading [47], as illustrated in Fig. 4(c). The torque-preloading relationship is often described by means of a constant K, known as the torque coefficient, as shown in Eq. (1) [48, 49].

$$T = K P_b d \tag{1}$$

In Eq. (1), T is the torque applied to the bolt head or nut, P_b is the preloading force and d is the nominal bolt diameter. For the FE analyses conducted herein, a value of 0.2 has been assigned to the torque coefficient K following the recommendations in [48, 49]. The bolt slip resistance for a given applied torque can be then calculated according to Eq. (2) [50], where μ is the friction coefficient (taken as 0.15 [47]) and n_b is the number of slip surfaces.

$$F_{slip} = \mu P_b n_b \tag{2}$$

For the numerical process, an initial step is to define the boundary conditions and contact pairs of the modelled connection. In the second step, bolt pretension force is applied using the Bolt Load command in ABAQUS [23], while in the following step(s), external loads are introduced

in the numerical models. The numerical simulations are performed using a dynamic implicit solver.

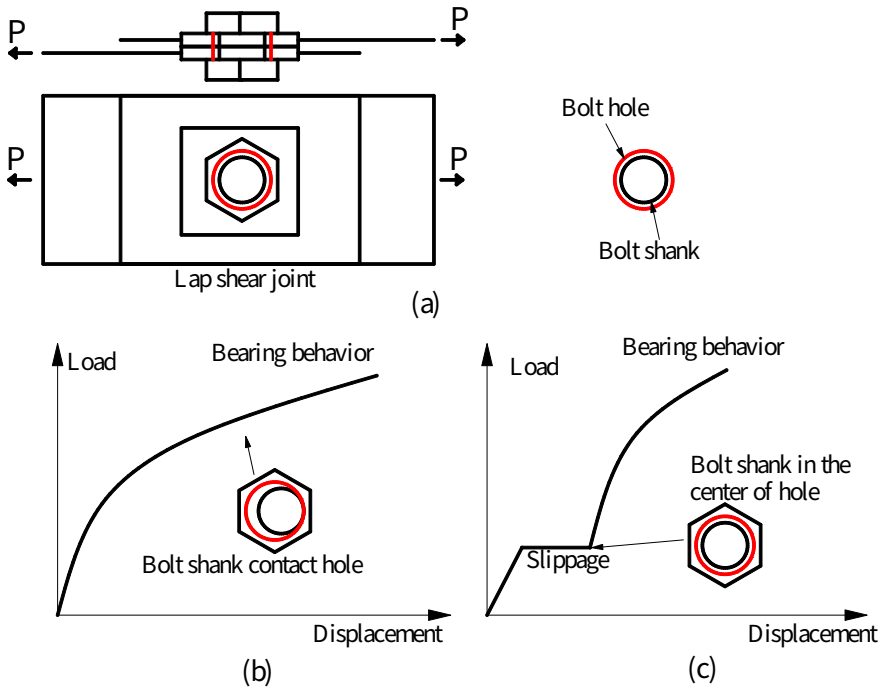

Fig. 4. Load-displacement curves for a lap shear joint loaded in tension (a) schematic of FE model; (b) load-displacement curve obtained from lap shear joint test in which clearance between bolt hole and bolt shank is eliminated prior to loading; and (c) load-displacement curve obtained from lap shear joint test in which clearance between bolt hole and bolt shank exists prior to loading, showing a bolt friction slippage mechanism

3 Validation of the proposed numerical method

The proposed numerical method has been validated against experiments on cold-formed steel connections reported in the literature [13, 18, 51]. The proposed numerical method was firstly examined against the bolted double shear-lap connection test, which was conducted under monotonic loading as reported by Lim and Nethercot [51]. The proposed numerical method

was then examined against a more complex test of CFS apex connections of an industrial portal frame, which was performed under monotonic loading conducted by Öztürk and Pul [51]. Furthermore, the tests of bolted gusset plate connections under both monotonic and cyclic loadings, carried out by Bagheri Sabbagh *et al*. [13], were used to examine the accuracy of the proposed modelling approach for simulating complicated contact problems under different loading conditions. The comparisons show that the proposed numerical method is capable of accurately simulating the structural behaviour of CFSstructures assembled using bolted connections. The demonstrated FE models in this section were programmed using Python of ABAQUS [46], facilitating the modelling and validation process.

3.1 CFS bolted double-shear lap connection

3.1.1 Tests by Lim and Nethercot [18]

A series of double-shear lap connection tests have been conducted by Lim and Nethercot [18]. The tests aimed to investigate the bolt hole elongation behaviour with an M16 bolt bearing against 3mm CFS plates, as detailed in Fig. 5. The test specimen of P1 by Lim and Nethercot [18] has been selected and simulated in the present study for validation purposes.

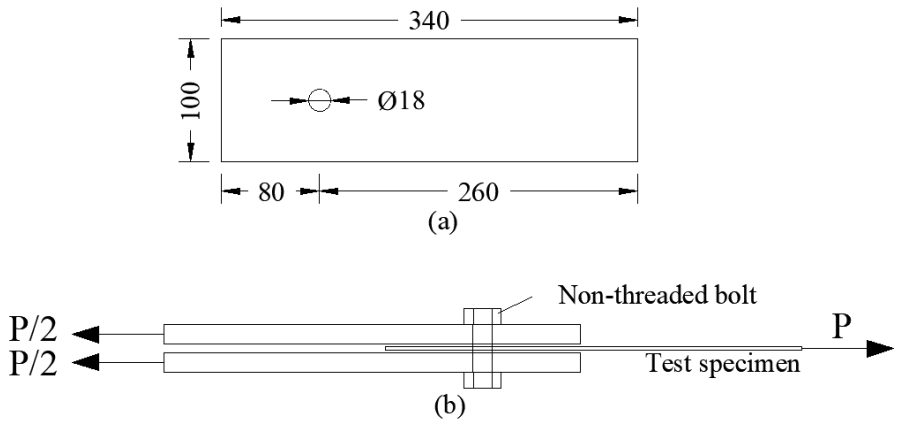

Fig. 5 Nominal dimensions of a double-shear lap test specimen of P1 [18]: (a) nominal dimensions of CFS plates and (b) schematic drawing of test

Fig. 6 illustrates the engineering stress-strain curve measured from the coupon test for the CFS plates [11] and the corresponding true stress-strain curves employed in the developed FE model. The engineering yield stress f_y, the ultimate engineering stress f_u and the strain at the ultimate engineering stress ε_u were 343 MPa, 431 MPa and 0.095, respectively. The Young's modulus *E* and the Poisson's ratio *v* were taken as 210 GPa and 0.3, respectively.

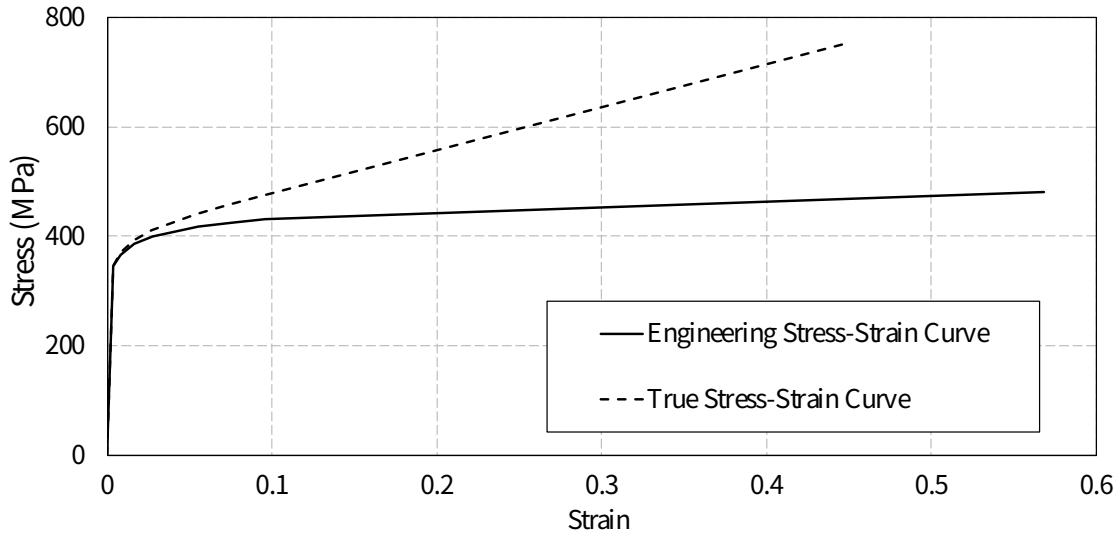

Fig. 6. True and engineering stress-strain curves for CFS plates [11].

3.1.2 Development of FE model

The FE model using the proposed modelling technique was developed to simulate the structural behaviour of the test lap shear connection of P1. Unless otherwise indicated, plain bolt shanks were modelled in all the FE analyses. The 4-noded quadrilateral S4R shell element [46] was employed for modelling the CFS plates away from the bolt holes. The 8-noded liner solid element C3D8R [46] was used to model the bolt and the block plates around the bolt hole. Surface-to-surface contacts were defined between the bolt and the contacted block plates, as well as between the contacted block plates modelled using the solid elements. Reference points were coupled to the nodes at the end section of the corresponding plate and boundary conditions were applied to the FE model via these reference points, as shown in Fig. 7. The meshes and

boundary conditions of the FE model are shown in Fig. 7. The bolt shank and plates were positioned to eliminate the clearance between the bolt and the bolt holes of the plates in the FE model as bolt slippage was not observed in the test load-deformation curve [18].

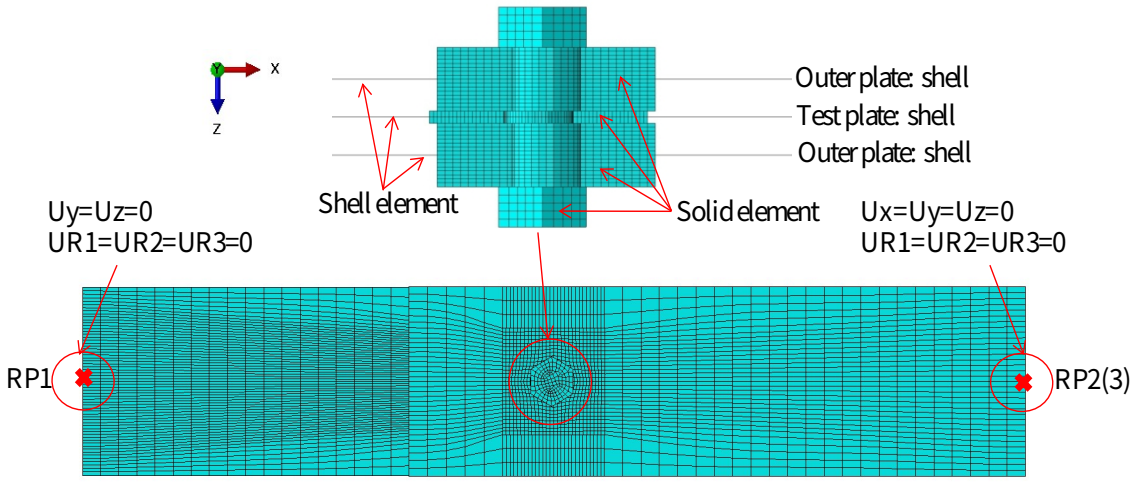

Fig. 7 FE model of double-shear lap test of P1 [18]

The true stress-strain curve as shown in Fig. 6, was employed to define the material properties of CFS test plate in the FE model, while material properties of the bolt and the hot-rolled outer plates were defined as elastic since these components remained elastic throughout the testing. The bolt pretension force was not applied in the FE model to be consistent with the test [18]. A displacement was applied to the reference point of RP1 to mimic the displacement-controlled loading scheme adopted in the connection test.

3.1.3 FE results and validation

The load-displacement curves obtained from the test and FE model are compared in Fig. 8. As shown in Fig. 8, the FE model using the proposed modelling technique yielded accurate predictions of the tested lap connection of P1 [18]. The Mises stress contours at different bolt hole elongations are shown in Fig. 9. Note that the unit of stresses shown in Fig. 9 is MPa and the grey areas represent locations where materials reach or exceed the yield strength. As can be observed in Fig. 9, the plastic region resulted from the bearing action extended rapidly

associated with significant in-plane deformations with the increase of the bolt hole elongation. Piling up of materials in the testing plate was also observed in the loading process. No convergence problem has been encountered during the FE calculation process.

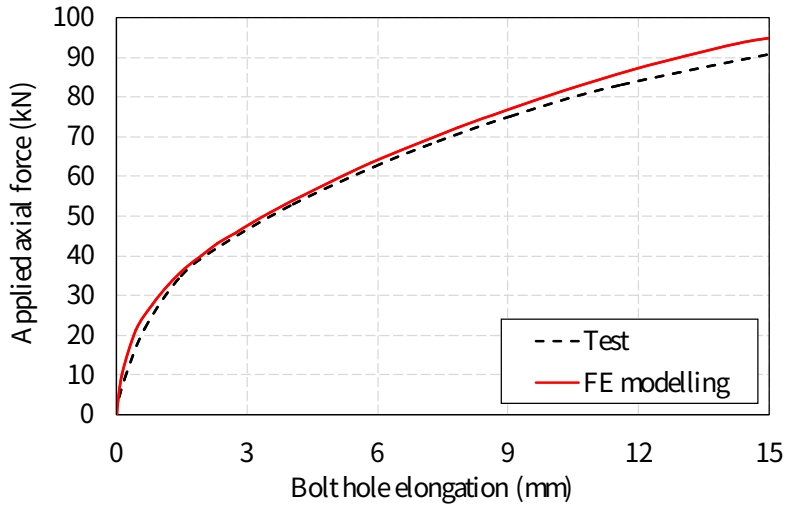

Fig. 8. Comparison between test and FE curves of the lap connection of P1 [18]

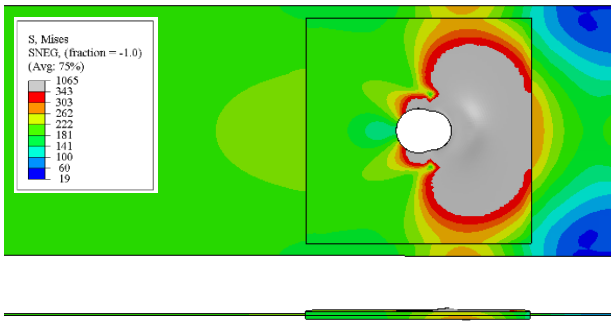

(a)

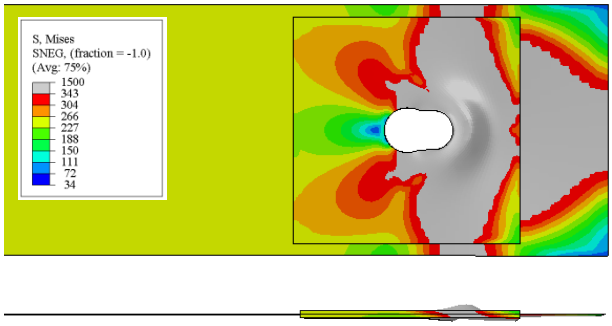

(b)

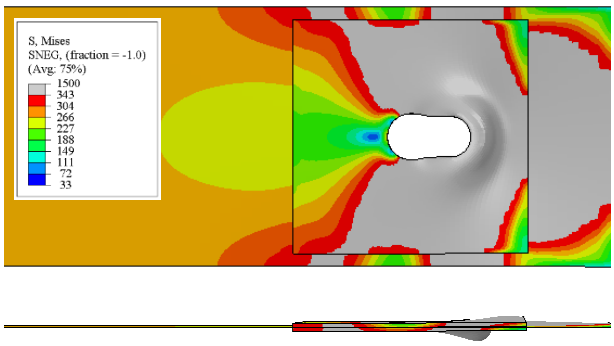

(c)

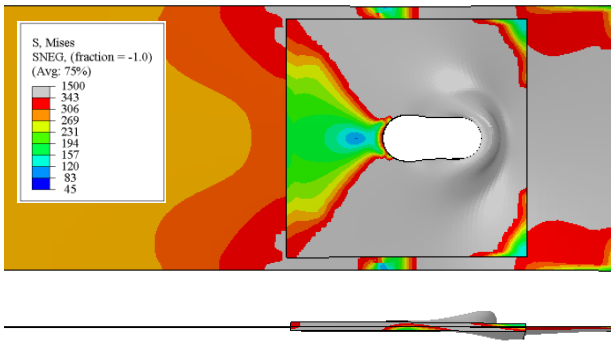

(d)

Fig. 9. Mises stress contours of the CFS plate at different bolt hole elongations: (a) bolt hole elongation of 5mm; (b) bolt hole elongation of 10mm; (c) bolt hole elongation of 15mm; and (d) bolt hole elongation of 20mm.

3.2 Full-scale apex connection tests by Öztürk and Pul [51]

Tests on apex connection of an industrial portal frame constructed with cold-formed back-to-back double sigma profile rafters were conducted by Öztürk and Pul [51]. The tests aimed to investigate local buckling behaviour and load-deformation behaviour of the apex plate under monotonic load. In this study, the proposed numerical approach was validated against the two tests of D360 and D360ST, as detailed in [51]. The connections were composed of 5 individual steel components which were assembled by 32 bolts. This validation aims to examine the robustness and efficiency of the proposed methodology in simulating CFS bolted connections with complicated configurations.

3.2.1 Test setup

Two tests on apex connections of an industrial portal frame, constructed with cold-formed back-to-back double sigma profile rafters of D360 and D360ST, respectively, have been conducted. The rafters were composed of an apex plate and back-to-back double sigma profiles. The detailed drawing of the test set-up and the specimen configurations of D360ST are shown in Fig. 10. Compared to the specimen of D360ST, there was no stiffener to the apex plate for D360, while other specimens and test set up were the same. Thirty-two M14-1.5 metric hex bolts of grade 8.8 were used in the apex connection. The loads were applied at the two points connected to the round bars, as indicated in Fig.10. The corresponding displacements at the round bars were measured by LVDTs.

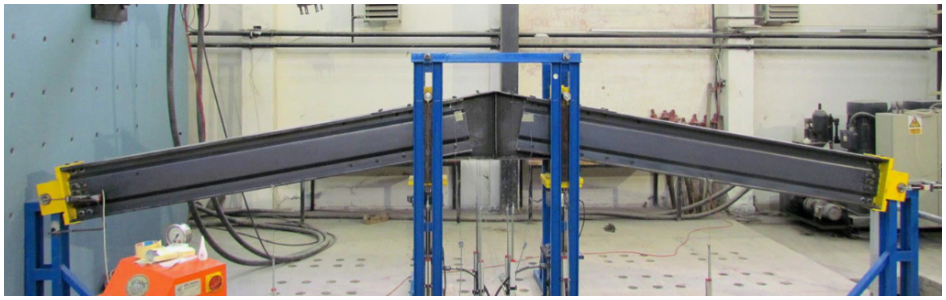

(a)

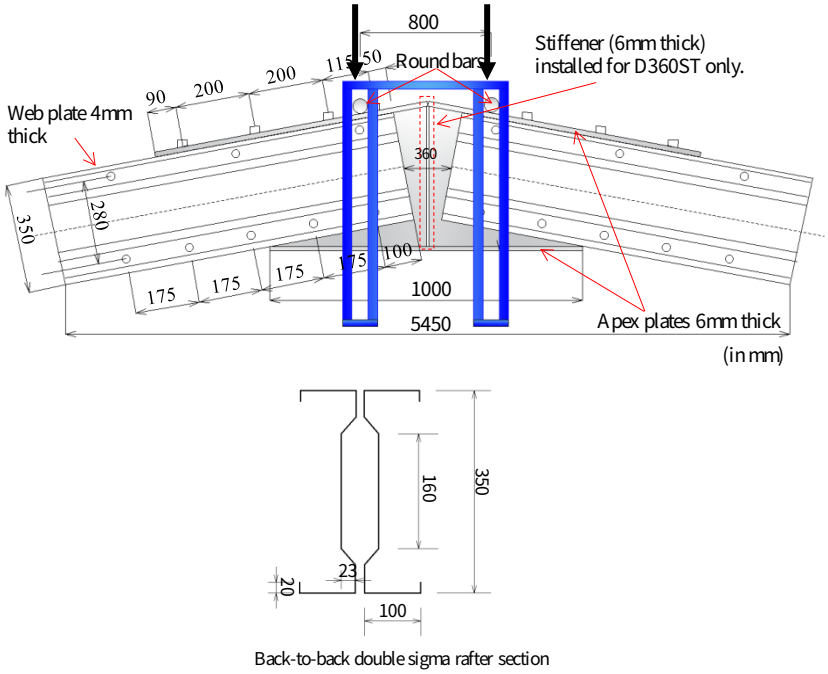

(b)

Fig. 10 Detailed drawing of D360ST: (a) test set up [51]; and (b) specimen configurations

3.1.2 Development of FE model

The FE models of the apex joints using the proposed methodology were validated against the test results reported in [51]. The two ends of the sigma profiles and one end surface of each round bar were coupled to reference points in all directions. Boundary conditions that allowed movement along Y-axis and rotation across Z-axis of the sigma profiles were applied to the reference points. The round bars were only allowed for the translational movement along the Y-axis to simulate the restraints provided by the out-of-plane reaction frames. These boundary conditions were achieved by applying the restraints to the reference points that were coupled

to the round bar surfaces. The peak point of the apex connection was restrained from movement along the X-axis due to symmetry. The meshes and boundary conditions of the developed FE models are presented in Fig. 11.

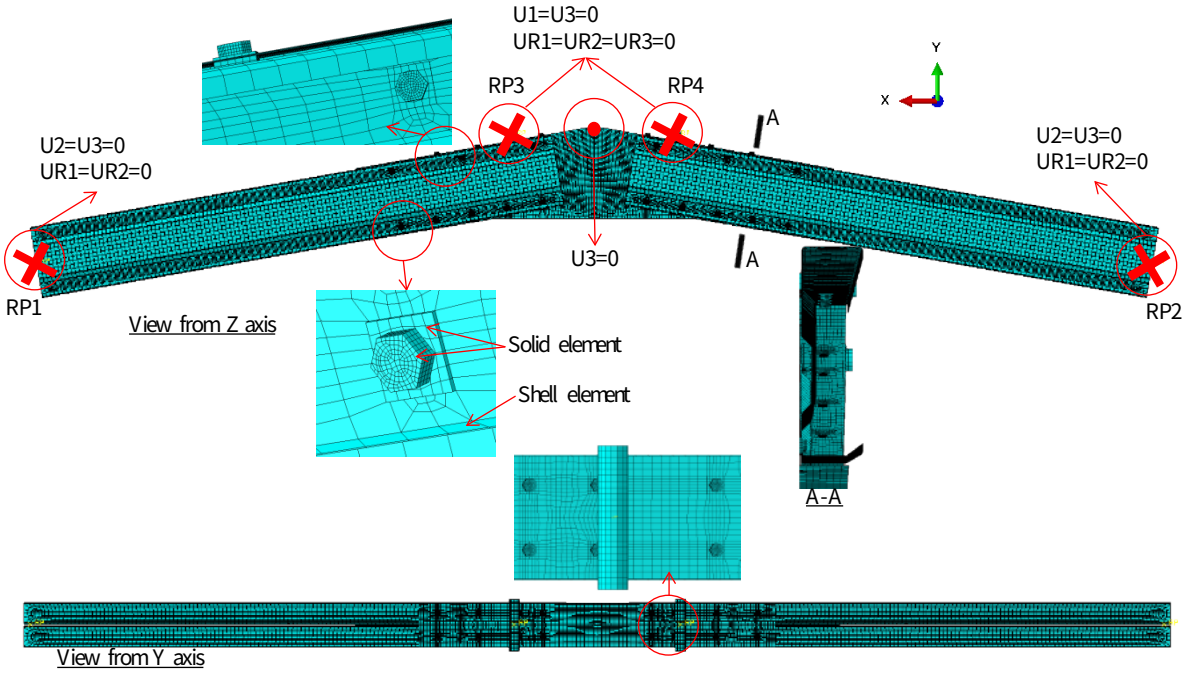

Fig. 11 Meshes and boundary conditions of the developed FE models

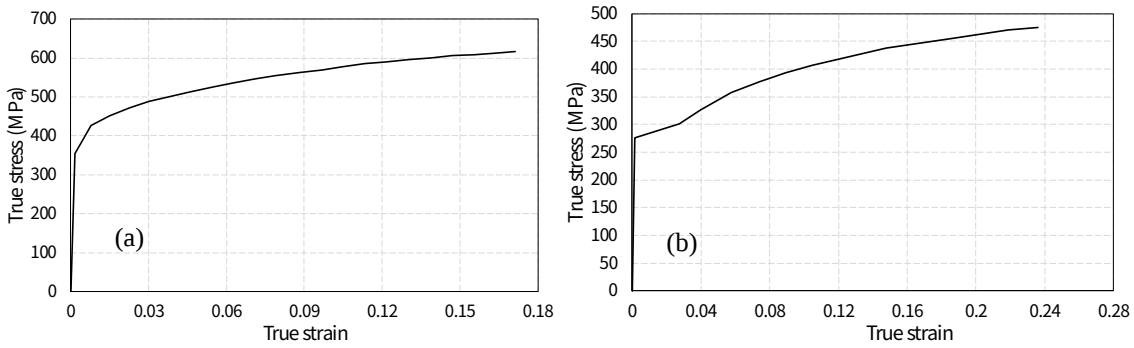

Fig. 12 True stress-strain curves for FE analysis obtained from [51]: (a) cold-formed steel channels; and (b) apex connecting plates

The 4-noded quadrilateral S4R shell element in ABAQUS [46] was employed for modelling all the cold-formed steel plates away from the bolt holes. The 8-noded liner solid element C3D8R [46] was used to model the round bars where loads were applied, the bolts and the

areas of the plates around the bolt holes. Surface-to-surface contacts were defined between the bolts and contacted plates, as well as between the plates. There was a $\pm$ 1.0 mm clearance between the bolt holes and the bolt shanks. The true stress-strain curve of the test plate given in [18] and shown in Fig. 12 was used for the shell elements of the apex plate and rafter profile in the FE models. The engineering yield stress and the engineering ultimate stress of the bolts were 640 MPa and 800 Mpa, respectively. The Young's Modulus of all the materials was taken as 210 GPa and the poison's ratio was taken as 0.3. The stress-strain relationships from coupon tests of the cold-formed steel channels and apex connecting plates for the FE analysis were presented in Fig. 12. The bolt pretension force of 34 kN as that measured in the connection tests was applied in the FE models. Displacement control of the reference points coupled to the round bars was used to apply external loads to the apex connections.

3.1.3 FE results and validation for apex connections

The load-displacement curves obtained from the tests and FE models are shown in Fig. 13, where the vertical axis load was taken as the sum of the two loads applied to the round bars while the displacement was taken as that obtained at one of the round bars. It can be observed that the FE models yield accurate predictions for both tested apex connections of the portal frame [51]. The comparisons between FE results and tests of apex connection D360ST were only presented to the displacement of 120 mm, which was the peak testing load of the connections. The drop of the peak load was due to fracture starting from the bottom bolt hole at the gusset plate, which is out of the scope of this paper. Overall, the initial stiffness and the load-deformation curves of the FE models show good agreement with those obtained from the tests.

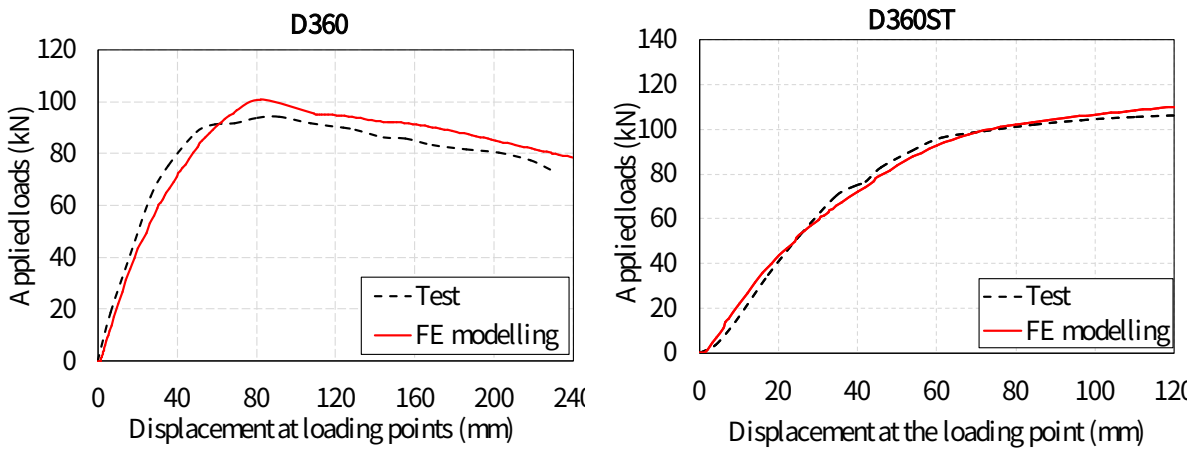

Fig. 13 Comparisons between test and FE curves of the apex connections D360 and D360ST

Comparisons of the deformation shapes between the tests and the FE modelling are shown in Fig. 14 and Fig. 15 for specimens of D360 and D360ST, respectively. It can be seen that the FE models are able to accurately capture the connection deformed shape, as well as the bolt hole elongations. This validation demonstrates that the FE models using the proposed numerical method are capable of modelling cold-formed steel connections with complex connection configurations (e.g. connections with a large number of bolts and substantial surface-to-surface contacts).

(a)

D360 D360ST

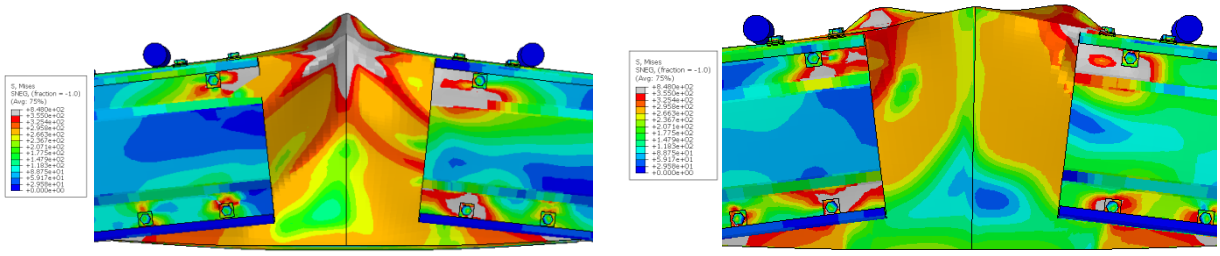

(b)

Fig. 14 Comparisons of the deformations shapes: (a) tests; and (b) FE modelling [51]

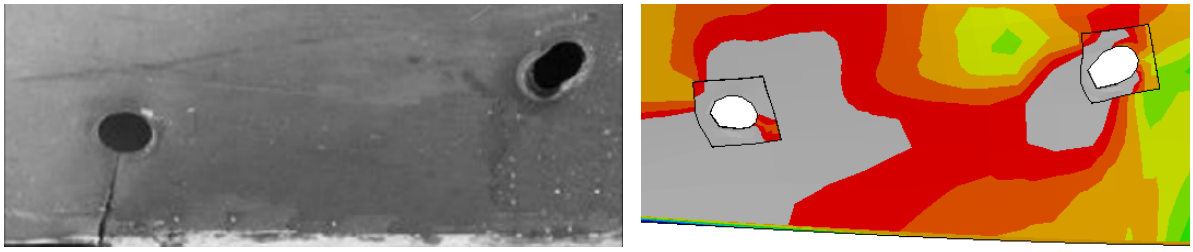

Fig. 15 Comparisons of the bolt hole elongation of D360ST [51]

3.3 Tests of bolted gusset plate connection by Bagheri Sabbagh *et al.* [13]

In this subsection, the proposed numerical approach is validated against the physical tests of a beam-to-column moment-resisting connection reported by Bagheri Sabbagh *et al.* [13]. The bolted connection was composed of 18 bolts in the back-to-back column and 16 bolts in the back-to-back beam. The beam and column were assembled using a gusset plate. The bolt torque was applied in the installation process which generated a pretension force at each bolt which was smaller than the critical slippage force as discussed in Section 2.3. As a result, bolt slippage was observed in the tests [13]. This validation aims to gain full confidence in using the proposed numerical approach to obtain the structural behaviour of complex connections, where complicated contact pairs and large rigid-body displacement (bolt slippage) exist under both monotonic and cyclic loadings.

3.3.1 Test set-up

In reference [13], the structural behaviour of cold-formed steel bolted moment-resisting connections subjected to cyclic loading was investigated. The moment resisting connection was composed of two hot-rolled steel channel columns, two cold-formed steel beams with curved flanges and a gusset plate used to connect the column and beams, as shown in Fig. 16. The variables adopted in the tests, which could have an influence on the structural earthquake-resistant mechanism, were the configurations of the out-of-plane stiffeners of the beams and the torques applied to the bolts which can result in different bolt pretension forces and, thus, different slippage behaviour of the connections.

In this study, the specimen B2 has been used to validate the proposed FE modelling methodology. Specimen B2 was dominated by rotational behaviour produced by connection slippage and bearing deformation in the bolts. The out-of-plane stiffeners were added in the vicinity of the connection to improve the strength and ductility of the full-scale connections [13]. The test set-up and the dimensions and configurations of the test specimens are shown in Fig. 16.

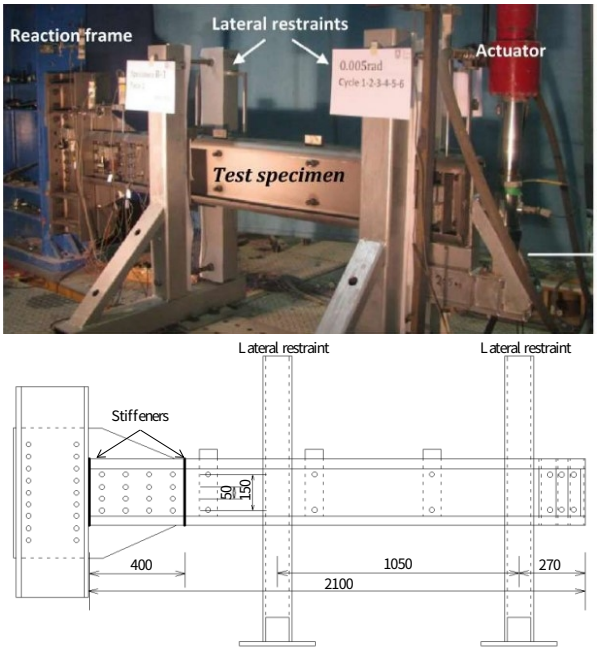

(a) (b)

Fig. 16 Test setup: (a) test specimen set-up [13]; and (b) dimensions and configurations of test specimen B2

3.3.2 Development of FE model

The FE model of the bolted gusset plate connection [13] is shown in Fig. 17. In the FE model, the 8-node linear solid element C3D8R in ABAQUS [46] was used to model the bolts and the plate components around and adjacent to the bolt holes. The general-purpose S8R element, which is an 8-noded quadrilateral shell element with reduced integration in the ABAQUS element library [46] was used to model the steel plates away from the bolt holes. A mesh size of the shell elements equal to approximately 20 mm was assigned uniformly to the FE model. It was observed that further refinement of the mesh did not result in any significant increase in the accuracy of predictions.

Suitable boundary conditions were employed in the FE model to simulate the test set-up of the connection [13]. The column was fixed at its top and bottom ends by setting Ux = Uy = Uz = 0 to the nodes at the end sections, as illustrated in Fig. 17. In the test setup, the beam end was constrained from the out-of-plane movement and the rotation along the longitudinal axis in order to prevent lateral-torsional buckling of the beam. In the FE model, this boundary condition was implemented by restraining the degrees of freedom of Ux=0 and UR2=0 at a reference point (RP), which was located within the end section and coupled to all the nodes at the end section, as shown in Fig. 17. The out-of-plane deformation of the beam was restrained by setting Ux = 0 to the nodes within the locations where lateral restraints were provided in the test [13], as shown in Fig. 17. A vertical displacement was applied to the reference point (RP) at the beam end. Surface-to-surface contacts were defined between the bolts and their contacted plates as well as between the plates modelled using the solid elements. The friction coefficient

of 0.3 was defined in the tangential direction while “hard contact” was defined in the normal direction of the contact pairs. Initial clearance of ±1mm between the bolt shank and the bolt hole was included in the FE model.

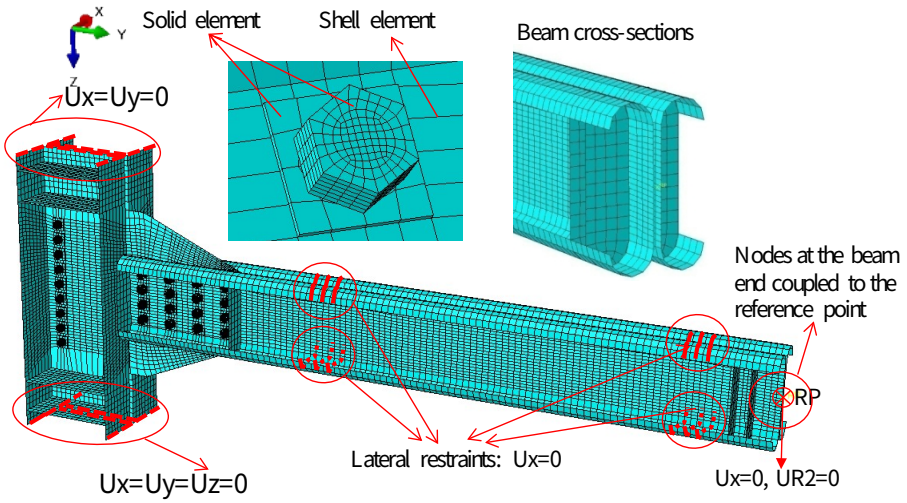

Fig. 17 FE model of the bolted beam-to-column connection B2 [13]

The true stress-strain curves of the beam and the gusset plate, given in [18] and shown in Fig. 18, were used to define the material properties of the shell elements of the corresponding component. The nonlinear true stress-strain curves from the tests were represented by the multi-linear curves before inputting into the FE model. No damage was observed in the overly designed column, therefore, the elastic material properties were used in the FE modelling for columns. The Young’s modulus of all the input materials was taken equal to 210 GPa while the poison’s ratio was taken as 0.3.

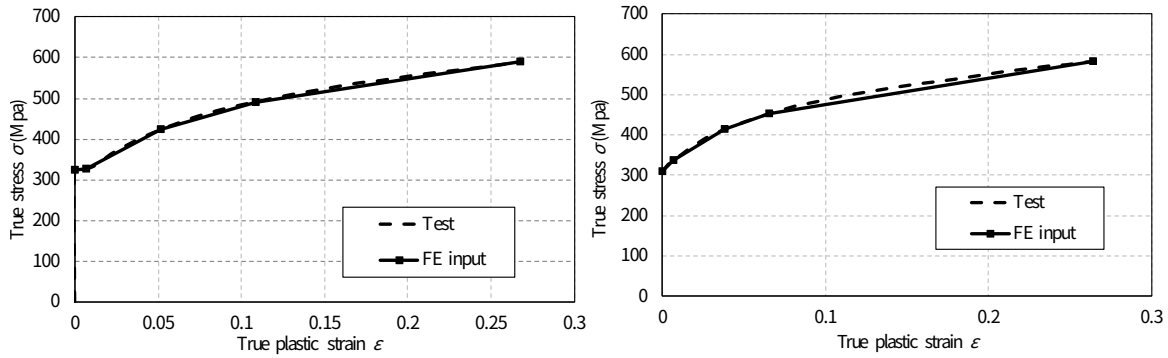

(a) (b)

Fig. 18. Ture stress-plastic strain relationships from (a) beam, and (b) gusset plate

Geometric imperfections were included by superimposing the magnified lowest buckling profile, obtained by conducting a prior buckling analysis, on the FE model. The magnitude of the imperfection was taken as $e = 0.2t\lambda_s$, where t is the thickness of the cold-formed steel element and λ_s is the cross-sectional slenderness [52].

In the FE model, a large pretension force of 80 kN was applied to each bolt at the column since a large bolt torque was applied in the installation of the connection [13]. The pretension force was greater than the critical slippage force, and consequently, the bolt slippage in the column of the connection was found to be negligible. The pretension force of bolts in the beam was varied as described in the following section. The dynamic implicit solver was employed to solve the model subjected to the cyclic loading. The displacement control scheme was employed to the reference point at the beam end section to mimic the cyclic loading of the test. The cyclic loading scheme used in the FE models (shown in Fig. 19) was identical to that used in the test [13].

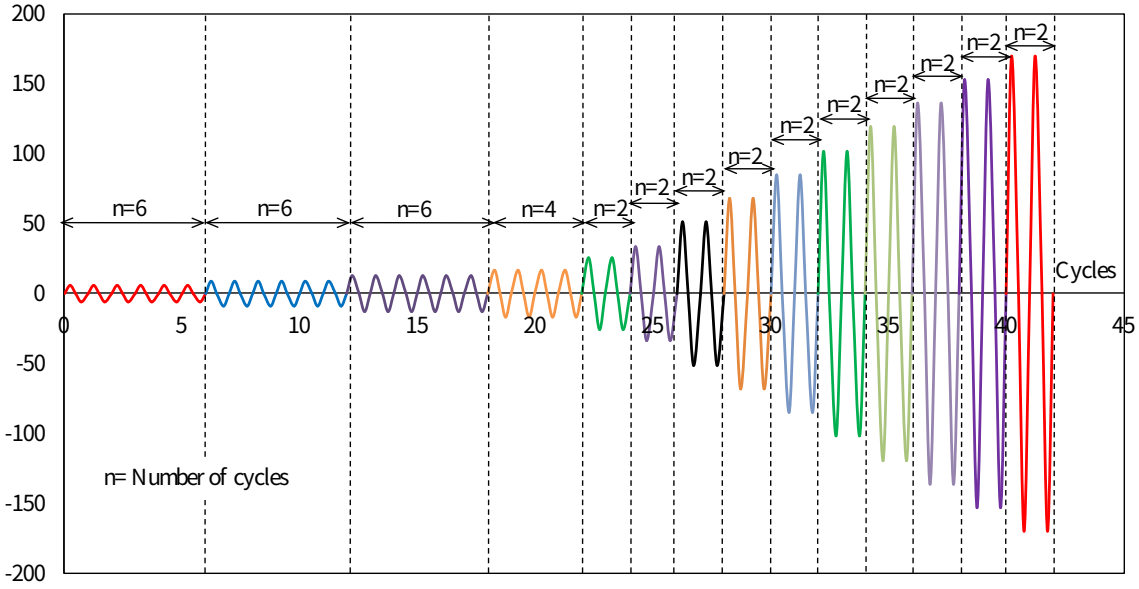

Fig. 19 Cyclic loading scheme adopted in the test and the FE model

3.3.3 FE results and validation

The comparison of the normalized moment (M/M_p)-rotation curves obtained from the FE analysis and the test [13] is shown in Fig. 20. M is the applied bending moment at the connection equal to the applied load multiplied by the cantilever length and M_p is the beam plastic moment resistance. The rotation of the connection is calculated by the vertical displacement at the beam end divided by the cantilever length. A pretension force of 15 kN [13] was applied to each bolt at the beam where a good agreement with the experimental results was obtained. It can be observed that the FE model yielded accurate predictions of the moment-rotation curves without essential test data from shear lap tests. The modelling method presented in Fig. 2 was used as input for the nonlinear connector elements to simulate the bolts.

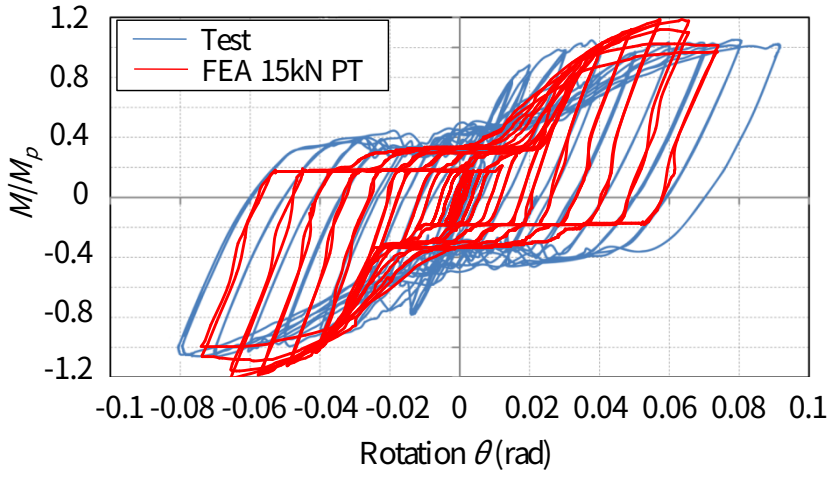

Fig. 20 Comparisons of the moment-rotation hysteretic curves between FE results and the tests with 15kN pretension force

The comparisons of the failure deformation modes at the final cycle of the test and the FE simulation are shown in Fig. 21. The plastic area was concentrated in the vicinity of the web stiffeners. It can be seen from Fig. 21 that the FE model can successfully replicate the observed

experimental responses where local buckling occurred at the web and bottom flange of the beam section located adjacent to the beam stiffeners.

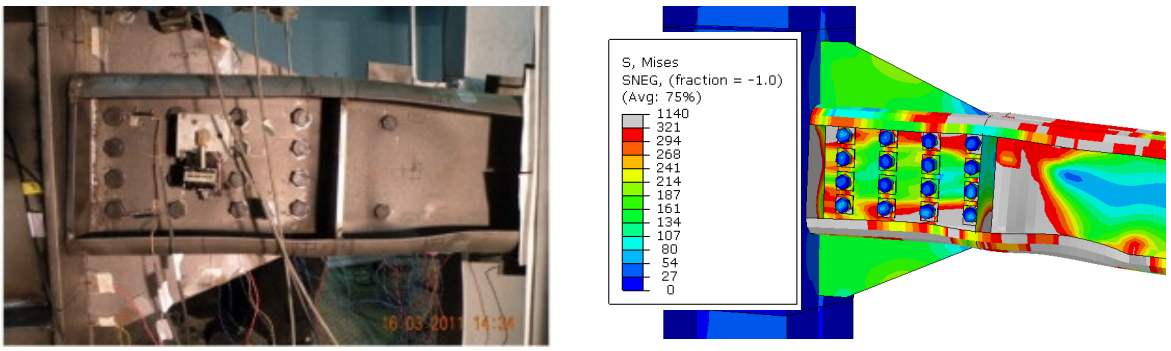

(a) (b)

Fig. 21 The failure deformations at the final cycle in the test and the FE analysis: (a) test, and (b) FE results

3.3.4 Further discussions

Fig. 22 shows the comparison of the FE results obtained based on different assumptions of the pretension force of the bolt at the beam. The pretension forces in the beam bolts were changed while the geometries, material properties and loadings remained the same. This can isolate the parameter of the pretension force and evaluate the effect of the bolt pretension force on the rotational behaviour of the bolted moment-resisting connections. As shown in Fig. 22 (a) and (b), when the applied pretension force of the beam bolts was relatively small, the overall structural behaviour of the full-scale connections was dominated by a connection slip-bearing action. However, when the pretension force of the beam bolts increased from 30 kN to 120 kN, the flexural deformation and the local buckling of the beam dominated the failure of the connection The proposed FE model of the beam-column connection was capable to simulate the influence of the bolt pretension force on the structural behaviour of the beam-column connection.

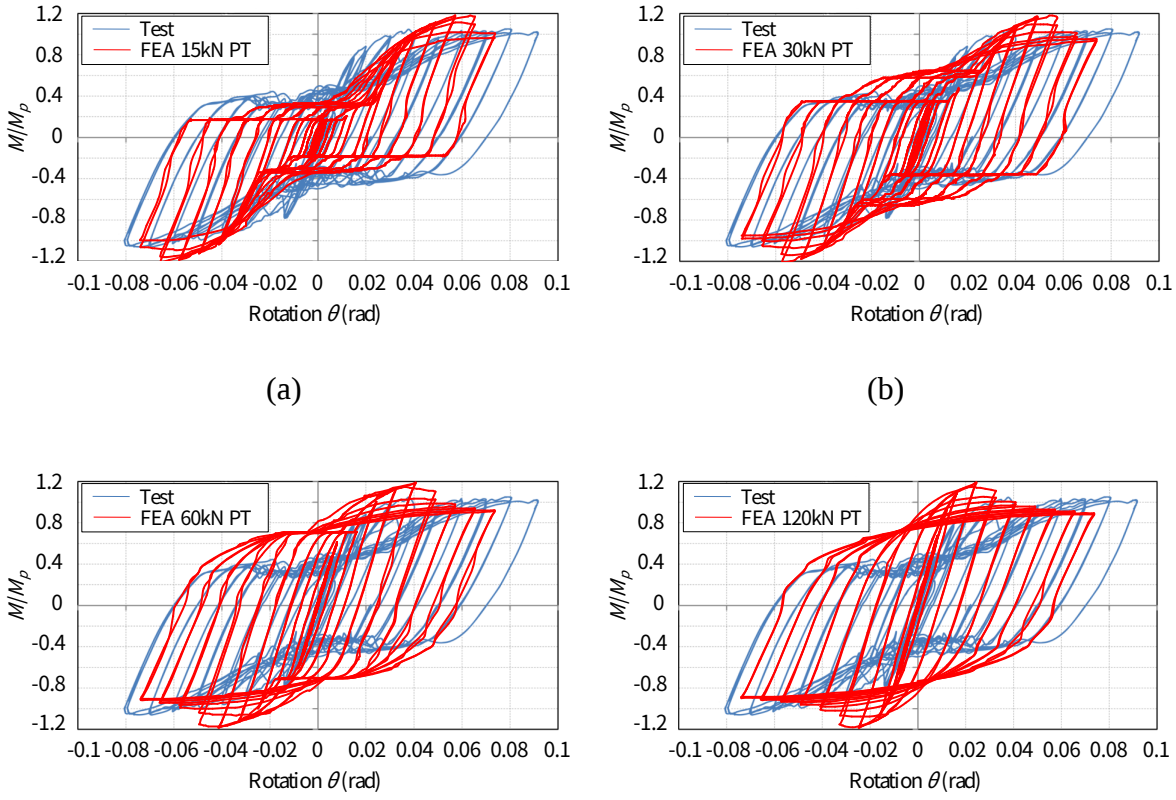

(a) (b)

(c) (d)

Fig. 22 Comparisons of the moment-rotation hysteretic curves between FEA and the tests with different pretension forces: (a) 15kN pretension, (b) 30kN pretension, (c) 60kN pretension, and (d) 120kN pretension

As one of the important advantages, the proposed methodology can autonomously model the bolting slip-bearing mechanism (Fig. 4), the influence of the bolt slippage is discussed here. The general flexural behaviour of a connection with and without bolting friction-slippage mechanism is shown in Fig. 23. The dashed line represents the connection moment-rotation relationship with bolt slippage mechanism. On the dashed line, during the first phase (O-A), the friction of the bolts are below the friction resistance and no bolting slippage occurs but there exist bearing force between the bolts and the plates. After Point A, when the bolt friction force reaches the friction resistance, slippage occurs in models in phase A-B. The total slippage in the connection is determined based on the summation of bolt holes clearance and elongation.

The bolt starts to bear against the steel plate again at point B. In the phase from B to C, connection rotation increases with the moment increasing up to the peak Point C, which is the connection moment capacity. In the final stage, the rotation keeps increasing while the moment decreases due to the local buckling of the beam.

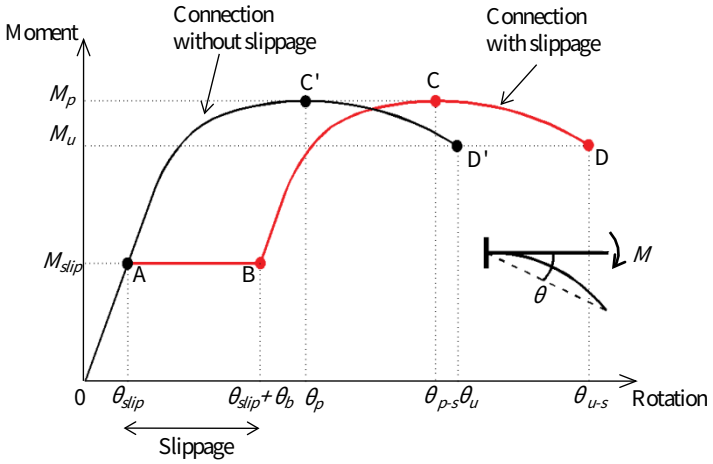

Fig. 23 General flexural behaviour of a connection with and without bolting friction-slip mechanism

Fig. 24 shows the comparisons of the moment-rotation curves from FE analysis with different pretension forces under monotonic loads. It can be seen that slippage occurs when M/M_p is equal to 0.17, 0.34 and 0.68 for applied bolt pretension forces of 15 kN, 30 kN and 60 kN, respectively. When the applied pretension force is 120 kN, no bolt slippage was observed according to Fig. 24. Fig. 24 also shows that the bolt slippage has a negligible effect on the connection moment capacity when the bearing deformation in the bolts was not significant (Fig. 25).

Fig. 24 Comparisons of the moment-rotation curve between FE analysis with different pretension forces under monotonic loads and the test [13]

The Von-Mises stress distribution for FE models under different pretension forces is shown in Fig. 25. For the models with bolt pretension force of 15 kN, 30 kN and 60 kN, it can be seen that bolt slippage can be obviously observed at the interface between the bolts and the contacted plates and as a result, the connections were dominated in a slip-bearing behaviour (Fig. 22). For the model with a bolt pretension force of 120 kN, there is no bolt slippage observed in the FE model. These observations are supported by the discussion above. For the FE models, the local buckling occurred at the bottom flange of the beam section adjacent to the beam stiffener, which was in good agreement with that observed in the test [13]. These can again prove the reliability of the proposed numerical modelling method on cold-formed steel bolted connections.

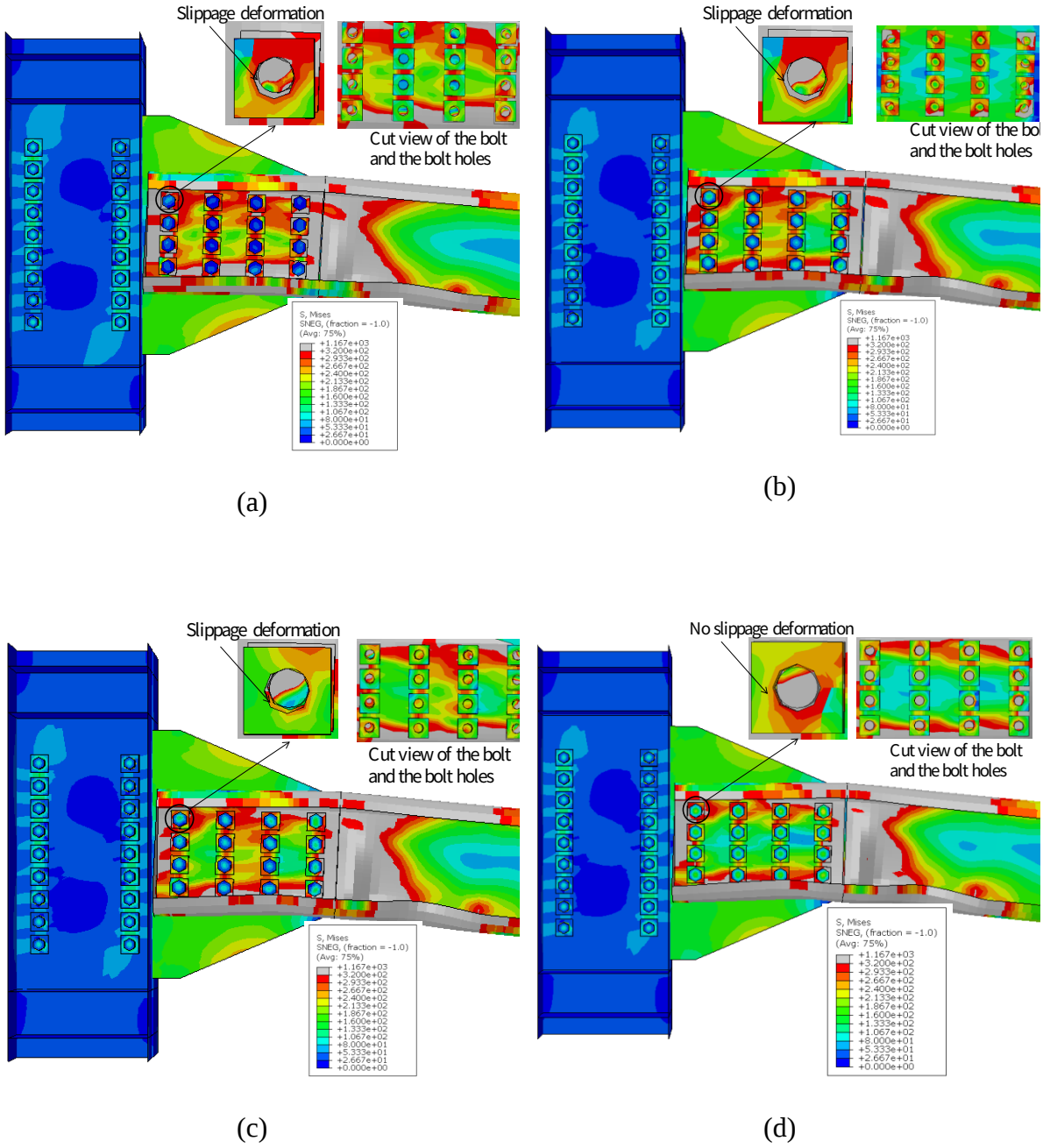

Fig. 25 Von-Mises stress distribution for FE models under different pretension forces: (a) pretension force = 15 kN; (b) pretension force = 30 kN; (c) pretension force = 60 kN; and (d) pretension force = 120 kN

4 Comparison of the spring/connector-based and the proposed approaches

The above section employed a lap joint test, a full-scale apex experiment and a bolted gusset plate connection cyclic test to validate the proposed numerical modelling technique. In this section, the double-shear lap connection test carried out by Lim and Nethercot [18] was used to examine the spring/connector-based numerical modelling technique as described in Section 1. The numerical results obtained from the spring/connector-based model (Fig. 26) were then compared with the results from the proposed numerical model (i.e. using both solid and shell elements). Note that the authors [16, 36-38] have successfully used the spring/connector-based model to simulate the structural behaviour of CFS bolted built-up beams and bolted connections subjected to both monotonic and cyclic loadings.

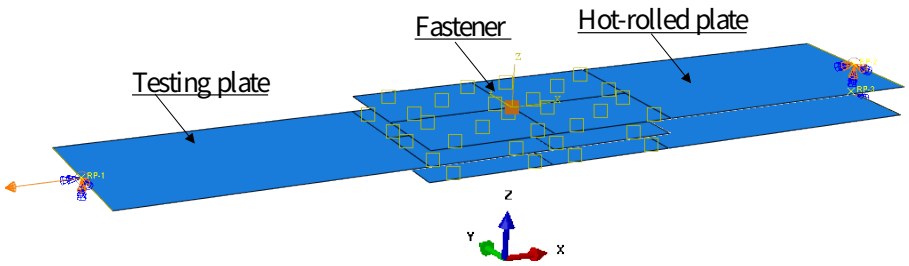

Fig. 26 Spring/connector-based numerical model of the double-shear lap connection [18]

The 4-noded quadrilateral S4R shell element in ABAQUS [46] was employed for modelling the plates in the lap joints. A mesh size approximately equal to 5 mm was assigned uniformly to the FE model, as shown in Fig. 27. Surface-to-surface contact pairs were defined between the contacted steel plates in the joint. Reference points were coupled to the nodes within the end edge of the corresponding plate and the boundary conditions were applied to the model via these reference points, as shown in Fig. 27.

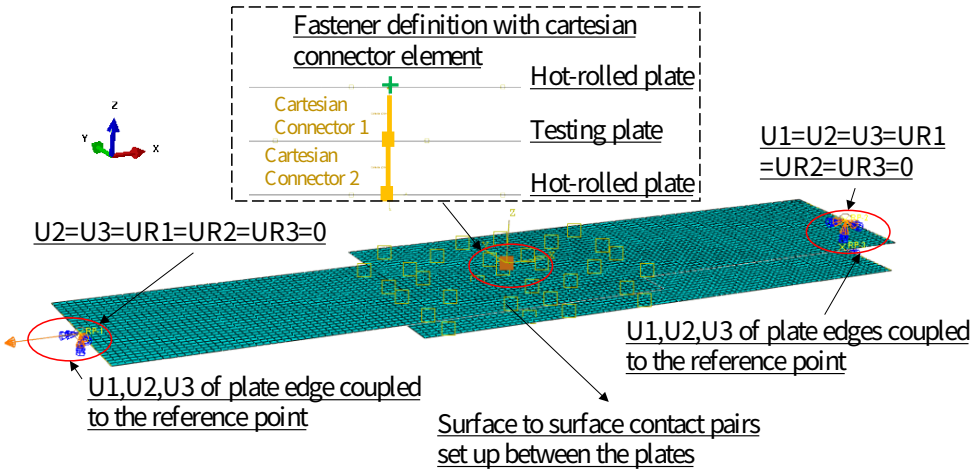

Fig. 27 FE modelling methodologies for CFS bolted connections using connector elements

The connector element of 'Fasteners' in ABAQUS [46] was used for the modelling of the bolt, as shown in Fig. 27. For the double shear test, a three-layer fastener configuration was used at the position of the bolt of the lap joint (see Fig. 27). The layer was connected by an anchored point with a physical radius in one plate and the other point with the same physical radius in the counterpart plate by means of a connector element. The behaviour of the connector element is directed defined via the force-deformation curves obtained from the tests, as shown in Fig. 28. This means tests or analytical equations are always needed when using the spring/connector-based modelling approach. The connector type of "Cartesian" with 3 relative translational degrees of freedom (U1, U2 and U3) was employed. This connector was characterised by a parallel combination of "Elasticity" and "Plasticity" behaviours, as defined in ABAQUS [46].]. It is noted that the behaviours of "Elasticity" and "Plasticity" are defined in the local coordinate system corresponding to the shear deformation of the bolts.

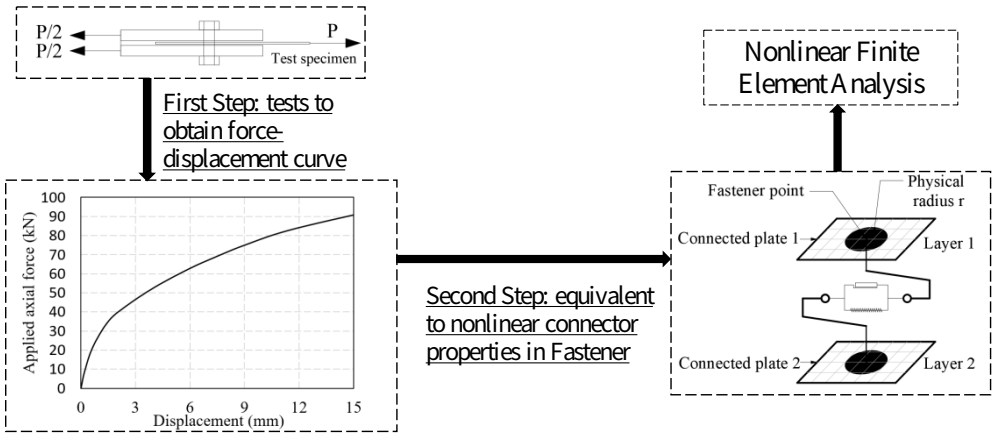

Fig. 28 Tests required for the connector-based modelling approach for CFS bolted connections

The bearing force-deformation relationship, which was obtained from the tests by Lim and Nethercot [18], was included in the connector element as shown in Fig. 28. It is important to evaluate the effect of bearing deformation resulted from the bearing of each end node of the connector element at the bolt position. In the Fastener definition, the “physical radius” in ABAQUS [46] was varied to examine the effects. Each end node of the connector element at the position of the bolts was thereby connected to the nearby nodes in the CFS steel plates within the physical radius and the nodes are coupled to the fastener points to uniformly distribute the forces, as described in Section 1 of this paper.

The non-linear engineering stress-strain property of the material was obtained from the tests [18] and the corresponding true stress-strain curves shown in Fig. 6 were employed in the developed FE model. A displacement of 15 mm was applied to the reference point shown in Fig. 26 and Fig. 27 to simulate the displacement-controlled loading scheme adopted in the lap joint test. The FE modelling results including the force-displacement curves and Mises stress contours are shown in Fig. 29 and Fig. 30, respectively.

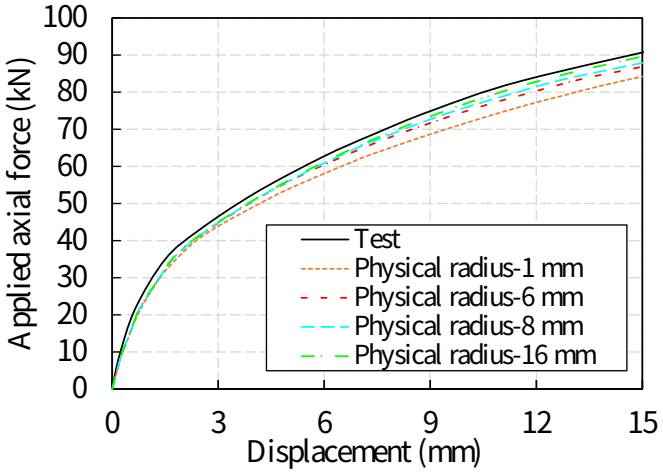

Fig. 29 Comparison of force-deformation curves obtained from the tests and the connector-based FE model with varing physical radii

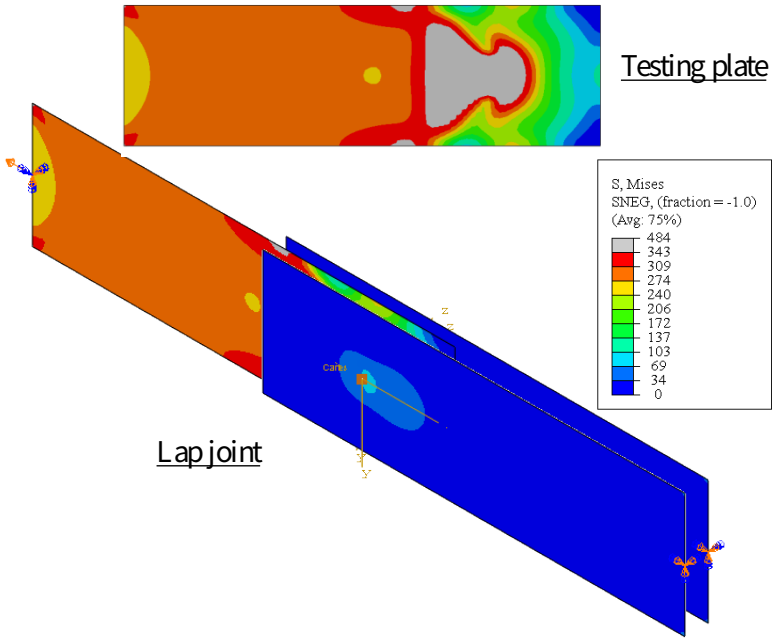

Fig. 30. Von Mises stress contours of the CFS plate at a displacement of 15 mm

The load-displacement curves obtained from the test and the connector-based model with varying physical radii of 1 mm, 6 mm, 8 mm and 16 mm, respective, are compared in Fig. 29. As shown in Fig. 29, the connector-based FE model produced slightly conservative predictions

of the stiffness and strength of the joint. This is because in this modelling approach, the endpoints of connector elements were coupled to their corresponding plate mesh nodes nearby the centre of bolt holes within a defined physical radius through the kinematic coupling, as illustrated in Fig. 2(c); the tensile deformation in the plates and the membrane deformation at the connector end led to an increased displacement thus a reduced stiffness prediction of the FE modelling, this in return supports the perspective pointed out by the authors in Section 1 and Section 2.

It can be seen from Fig. 30 that the connector-based numerical model fails to accurately capture the stresses development of the tested lap connection, especially for those located near the bolt holes. As can be observed in Fig. 9, the plastic region resulted from the bearing action is smaller than the results presented in Section 3.1.3. Piling up of materials were also not observed in the loading process due to a lack of bolt hole in the connector-based joint modelling. Given the high computational efficiency of connector-based FE modelling, it can be useful when tests of lap joints are given and the localised deformation and stresses are not the research focus. However, when physical lap tests (i.e. input parameters for the spring/connector elements) are impractical or unavailable, the proposed method using both shell and solid elements can be employed to accurately capture the structural behaviour of different CFS bolted connections.

5 Conclusions

Modelling CFS bolted connections can be a challenging task due to their complex structural behaviour associated with material nonlinearities, bearing failure, bolt slippage and surface-to-surface contacts. In this paper, a robust numerical approach that can accurately replicate the behaviour of thin-walled bolt connections, explicitly considering the bearing damage and other influencing factors such as the bolt slippage and bolt preloading, has been proposed. The proposed numerical modelling technique adopts the shell elements to model the majority parts

of CFS plates, while areas around the bolt holes of CFS plates as well as bolts are simulated using solid elements; this enables the establishment of accurate contacts between the bolt and contacted CFS plates as well as between contacted CFS plates, thus leading to accurate simulation results. It has been suggested that, for typical steel connections, an implicit dynamic analysis can ensure a robust and stable response. The proposed numerical approach has been validated against a number of CFS connections with different levels of complexity conducted by various researchers in both monotonic and cyclic loading schemes.

The comparisons show that the proposed numerical approach can accurately and robustly capture the structural behaviour of CFS connections, including both the bolt slippage and bolt bearing mechanism. The proposed approach can also be used in the simulation of CFS structures assembled using bolted fasteners at the structural level as the approach shows computational efficiency, simulation accuracy and ease of convergence. Furthermore, the application of this approach can be extended to the simulation of other types of CFS structures assembled using different types of fasteners.

References

[1] CEN/EN Eurocode 3, Part 1-3: Design of steel structures: General rules-Supplementary rules for cold-formed members and sheeting. European Committee for Standardization, Brussels;2006.

[2] AISI. North American specification for the design of cold-formed steel structural members. American Iron & Steel Institute, Committee of Steel Plate Producers; 2007.

[3] AS/NZS 4600: Cold-formed Steel Structures. Standards Australia Sydney, Australia; 2018.

[4] Quan G, Ye J, Li W. Computational modelling of Cold-formed steel lap joints with screw fasteners. Structures. 2021;33:230-45.

[5] Huynh MT, Pham CH, Hancock GJ. Experimental behaviour and modelling of screwed connections of high strength sheet steels in shear. Thin-Walled Structures. 2020;146:106357.

[6] Truong AN, Pham CH, Hancock G. Power-Actuated Fasteners Connecting High-Strength Steel Plate to Mild Steel Plate under Monotonic Shear Loading. Journal of Structural Engineering-ASCE. 2020;146:04020193.

[7] Truong AN, Pham CH, Hancock GJ. Power-Actuated Fasteners Connecting Cold-Formed Sheet Steels under Monotonic Tension Loading. Journal of Structural Engineering-ASCE. 2021;147:04020361.

[8] Truong AN, Pham CH. Numerical modelling of power-actuated fastener connections joining high-strength steel sheet to mild steel plate subjected to monotonic shear. Thin-Walled Structures. 2021;165:107950.

[9] Atia MKS, Jain MK. Finite element analysis of material flow in die-less clinching process and joint strength assessment. Thin-Walled Structures. 2018;127:500-15.

[10] Lim JB, Nethercot DA. Ultimate strength of bolted moment-connections between cold-formed steel members. Thin-Walled Structures. 2003;41:1019-39.

[11] Ho H, Chung K. Experimental investigation into the structural behaviour of lapped connections between cold-formed steel Z sections. Thin-Walled Structures. 2004;42:1013-33.

[12] Pham CH, Davis AF, Emmett BR. Numerical investigation of cold-formed lapped Z purlins under combined bending and shear. Journal of Constructional Steel Research. 2014;95:116-25.

[13] Sabbagh AB, Petkovski M, Pilakoutas K, Mirghaderi R. Experimental work on cold-formed steel elements for earthquake resilient moment frame buildings. Engineering Structures. 2012;42:371-86.

[14] Sabbagh AB, Petkovski M, Pilakoutas K, Mirghaderi R. Cyclic behaviour of bolted cold-formed steel moment connections: FE modelling including slip. Journal of Constructional Steel Research. 2013;80:100-8.

[15] Sato A, Uang C-M. Seismic design procedure development for cold-formed steel–special bolted moment frames. Journal of Constructional Steel Research. 2009;65:860-8.

[16] Ye J, Mojtabaei SM, Hajirasouliha I. Seismic performance of cold-formed steel bolted moment connections with bolting friction-slip mechanism. Journal of Constructional Steel Research. 2019;156:122-36.

[17] Rogers C, Hancock G. Bolted connection design for sheet steels less than 1.0 mm thick. Journal of Constructional Steel Research. 1999;51:123-46.

[18] Lim JB, Nethercot D. Stiffness prediction for bolted moment-connections between cold-formed steel members. Journal of Constructional Steel Research. 2004;60:85-107.

[19] Zaharia R, Dubina D. Stiffness of joints in bolted connected cold-formed steel trusses. Journal of Constructional Steel Research. 2006;62:240-9.

[20] Parastesh H, Mobedi E, Ghasemi H, Amjadiyan K. Experimental Study for Strength Capacity of Cold-Formed Steel Joists Connections with Consideration of Various Bolts Arrangements. Journal of Rehabilitation in Civil Engineering. 2019;7:101-14.

[21] Zadanfarrokh F, Bryan E. Testing and design of bolted connections in cold formed steel sections. 11th International Specialty Conference on Cold-Formed Steel Structures. Missouri University of Science and Technology;1992.

[22] Cai Y, Young B. Structural behavior of cold-formed stainless steel bolted connections. Thin-Walled Structures. 2014;83:147-56.

[23] Cai Y, Young B. Carbon steel and stainless steel bolted connections undergoing unloading and re-loading processes. Journal of Constructional Steel Research. 2019;157:337-46.

[24] Wang Z, Wang Y, Yun X, Zhang Y, Li Z, Wang Z. Numerical modelling of extruded aluminium alloy T-stubs connected by swage-locking pins: FE validation and parametric study. Thin-Walled Structures. 2020;155:106926.

[25] Salih E, Gardner L, Nethercot D. Numerical investigation of net section failure in stainless steel bolted connections. Journal of Constructional Steel Research. 2010;66:1455-66.

[26] Salih E, Gardner L, Nethercot D. Bearing failure in stainless steel bolted connections. Engineering Structures. 2011;33:549-62.

[27] Li L-Z, Liu X, Luo Y, Su M-N, Zhu J-H. Flexural Performance of Bolted-Side-Plated Reinforced Concrete Beams with Buckling Restraining. ACI Structural Journal. 2019.

[28] dos Santos JdJ, Liang Y, Zhao O, de Andrade SA, de Lima LR, Gardner L et al. Testing and design of stainless steel staggered bolted connections. Engineering Structures. 2021;231:111707.

[29] Yun X, Gardner L. Numerical modelling and design of hot-rolled and cold-formed steel continuous beams with tubular cross-sections. Thin-Walled Structures. 2018;132:574-84.

[30] Yun X, Gardner L. The continuous strength method for the design of cold-formed steel non-slender tubular cross-sections. Engineering Structures. 2018;175:549-64.

[31] Schafer BW, Li Z, Moen CD. Computational modeling of cold-formed steel. Thin-Walled Structures. 2010;48:752-62.

[32] Fontana M. Load-bearing and deformation behaviour of truss joints using thin-walled pentagon cross-sections. Thin-walled structures. 2004;42:295-307.

[33] Yu W, Chung K, Wong M. Analysis of bolted moment connections in cold-formed steel beam–column sub-frames. Journal of Constructional Steel Research. 2005;61:1332-52.

[34] Shi Y, Wang M, Wang Y. Analysis on shear behavior of high-strength bolts connection. International Journal of Steel Structures. 2011;11:203-13.

[35] Blum H, Rasmussen K. Experimental and numerical study of connection effects in long-span cold-formed steel double channel portal frames. Journal of Constructional Steel Research. 2019;155:480-91.

[36] Ye J, Mojtabaei SM, Hajirasouliha I, Shepherd P, Pilakoutas K. Strength and deflection behaviour of cold-formed steel back-to-back channels. Engineering Structures. 2018;177:641-54.

[37] Ye J. More efficient cold-formed steel elements and bolted connections: University of Sheffield; 2016.

[38] Ye J, Mojtabaei SM, Hajirasouliha I, Pilakoutas K. Efficient design of cold-formed steel bolted-moment connections for earthquake resistant frames. Thin-Walled Structures. 2019.

[39] Shahini M, Sabbagh AB, Davidson P, Mirghaderi R. Development of cold-formed steel moment-resisting connections with bolting friction-slip mechanism for seismic applications. Thin-Walled Structures. 2019;141:217-31.

[40] Wald F, Vild M, Kuříková M, Kabeláč J, Sekal D, Maier N et al. Component based finite element design of steel joints. Civil Engineering Design. 2020;2:78-89.

[41] Wald F, Šabatka L, Kabeláč J, Kolaja D, Pospíšil M. Structural Analysis and Design of Steel Connections Using Component Based Finite Element Model (CBFEM). Journal of Civil Engineering and Architecture. 2015;9:895-901.

[42] Šabatka L, Wald F, Kabeláč J, Gödrich L, Navrátil J. Component based finite element model of structural connections. Proceedings of the 12th International Conference on Steel, Space & Composite Structures. Czech Technical University in Prague;2014.

[43] Gödrich L, Wald F, Kabeláč J, Kuříková M. Design finite element model of a bolted T-stub connection component. Journal of Constructional Steel Research. 2019;157:198-206.

[44] Vild M, Kabeláč J, Kuříková M, Wald F. Design of gusset plate connection with single-sided splice member by component based finite element method. Structural Stability Research Council (SSRC); 2019.

[45] Kuříková M, Wald F, Kabeláč J. Design of slender compressed plates in structural steel joints by component based finite element method. SDSS 2019-International Colloquium on Stability and Ductility of Steel Structures;2019.

[46] Abaqus/CAE User's Manual. 2020.

[47] Winter G. Tests on bolted connections in light gage steel. Journal of the Structural Division-ASCE. 1956;82:1-25.

[48] Juvinall RC, Marshek KM. Fundamentals of machine component design: John Wiley & Sons New York; 2006.

[49] Bickford JH. An introduction to the design and analysis of bolted joints: Marcel Dekker, New York; 1997.

[50] Wong MF, Chung KF. Structural behaviour of bolted moment connections in cold-formed steel beam-column sub-frames. Journal of Constructional Steel Research. 2002;58:253-74.

[51] Öztürk F, Pul S. Experimental and numerical study on a full scale apex connection of cold-formed steel portal frames. Thin-Walled Structures. 2015;94:79-88.

[52] Dawson RG, Walker AC. Post-buckling of geometrically imperfect plates. Journal of the Structural Division-ASCE. 1972;98:75-94.